SCIENCE CHINA
Physics, Mechanics & Astronomy

•Article•

January 2025 Vol. 68 No. 1: 214311
https://doi.org/10.1007/s11433-024-2496-9

Merging bound states in the continuum in an open acoustic resonator

Lujun Huang[1*†], Bin Jia[2†], Artem S. Pilipchuk[3†], Sibo Huang[2], Chen Shen[4], Almas F. Sadreev[3*], Yong Li[2*], and Andrey E. Miroshnichenko[5*]

[1] *School of Physics and Electronic Sciences, East China Normal University, Shanghai 200241, China;*
[2] *Institute of Acoustics, Tongji University, Shanghai 200092, China;*
[3] *L. V. Kirensky Institute of Physics, Krasnoyarsk 660036, Russia;*
[4] *Department of Mechanical Engineering, Rowan University, Glassboro 08028, USA;*
[5] *School of Engineering and Technology, University of New South Wales at Canberra, ACT 2610, Australia*

Received May 17, 2024; accepted September 10, 2024; published online November 8, 2024

Bound states in the continuum (BICs) are perfectly localized resonances despite embedding in the continuum spectrum. However, an isolated BIC is very sensitive to the structure perturbation. Here, we report merging acoustic BICs in a single open resonator, robust against the structure perturbation. We find that both symmetry-protected BIC and Friedrich-Wintgen BIC are sustained in a single coupled waveguide-resonator system. By varying the height and length of the resonator, these two BICs move toward each other and merge into a single one at a critical dimension. Compared to an individual BIC, the merged BIC is robust against fabrication error because its Q-factor is proportional to ΔL^{-4}, where ΔL embodies the structure perturbation. The essence of this extraordinary phenomenon is perfectly explained by the two- and three-level approximations of the effective non-Hermitian Hamiltonian. Finally, we present direct experimental demonstrations of the moving and merging of BICs in a coupled 3D waveguide-resonator, which are evidenced by the vanishing of the linewidth of Fano resonance in the transmission spectra. Our results may find exciting applications in designing high-quality acoustic sources, sensors and filters.

acoustic resonances, bound state in the continuum, high-Q resonances

PACS number(s): 43.20.+g, 43.55.+p, 43.40+s

Citation: L. Huang, B. Jia, A. S. Pilipchuk, S. Huang, C. Shen, A. F. Sadreev, Y. Li, and A. E. Miroshnichenko, Merging bound states in the continuum in an open acoustic resonator, Sci. China-Phys. Mech. Astron. **68**, 214311 (2025), https://doi.org/10.1007/s11433-024-2496-9

1 Introduction

Bound states in the continuum (BICs), also known as trapped modes with an infinite quality factor (Q-factor), have triggered extensive interest in photonic and acoustic communities [1-10]. The most straightforward mechanism of BICs is the symmetrical incompatibility of the eigenstates of a closed system states with propagating states of the continuum, named symmetry-protected (SP) BICs. That results in a zero coupling of the eigenmode of the closed system with a propagating mode of the continuum [11-14]. The SP BICs were also found in a two-dimensional (2D) directional waveguide with symmetrically loaded rigid circular obstacles [15]. Recently, Jia et al. [16] found that SP BICs can be supported in a coupled waveguide-resonator system as long as the projected-plane symmetry is preserved.

*Corresponding authors (Lujun Huang, email: ljhuang@phy.ecnu.edu.cn; Almas F. Sadreev, email: almas@tnp.krasn.ru; Yong Li, email: yongli@tongji.edu.cn; Andrey E. Miroshnichenko, email: andrey.miroshnichenko@unsw.edu.au)
†These authors contributed equally to this work.

© Science China Press 2024

Another type of BICs is Friedrich-Wintgen (FW) BICs [2,17,18]. The formation mechanism of FW BICs can be attributed to the destructive interference between two modes [17,19,20], each of which is coupled with the continuum. The FW BICs can be realized in an open resonator by gradually changing the aspect ratio of the resonator when a degeneracy of eigenfrequencies occurs[18]. In acoustic systems, the FW BICs were proven to exist by many researchers [21-26]. The experimental evidence for the FW BICs was reported by Lepetit and Kanté [27] and by Huang et al. [28] in the most straightforward configuration of a rectangular resonator opened to one attached waveguide.

Less obvious types but similar to the SP BICs are the accidental BICs despite the absence of symmetry arguments. The coupling between the cavity eigenmode and the mode of the continuum can turn to zero accidentally by the variation of the shape of the cavity as it was demonstrated in an open Sinai billiard [29]. Such BICs were proposed by Friedrich and Wintgen [30] in their paper on the physical realization of BICs by placing a hydrogen atom in a magnetic field. Later, accidental BICs were demonstrated in photonic [31-34] and acoustic systems [25].

Although last ten years have witnessed rapid progress in photonic BICs, acoustic BICs have been hindered by the challenge of practical fabrication. Thanks to the advances in three-dimensional (3D) printing technology, acoustic metamaterials and metasurfaces can be easily fabricated [35,36], providing unprecedented freedom of manipulating acoustic wave propagation. Different acoustic resonances [8,37], including Mie resonances [38,39] and membrane resonances [40], have been demonstrated experimentally. Most of the published research works focus on acoustic resonances with relatively low-Q factors. Low-Q resonances are promising for realizing broadband sound absorption [41,42]. High-Q acoustic resonances, however, are less explored. As an unique resonance, acoustic BICs have infinite Q-factors and extreme sound trapping capability, thus providing an excellent way of realizing high-Q acoustic resonances. Recently, different types of BICs have been theoretically proposed [23,43-45] and experimentally realized [16,25,26,28,46,47]. The largest measured Q-factor based on quasi-BICs was reported to be 583 [28]. Notably, a high-Q quasi-BIC is usually accompanied by the giant near field enhancement, thus holding great promise in enhancing wave-matter interactions, such as ultra-narrowband absorbers [26,48], acoustic sources [49] (i.e., sound laser), and filters.

More recently, merging BICs has attracted considerable attention because they are robust against fabrication imperfections, providing an excellent solution for realizing ultrahigh-Q resonances. They have been successfully realized theoretically and experimentally in the context of dielectric grating [50-53], a chain of dielectric spheres and disks [54,55], and photonic crystal slabs [56-60]. However, most of the reported merging BICs take place in the momentum space by leveraging periodic structures. A recent work shows that such merging BICs can be achieved in a coupled resonator-waveguide system, where two Fabry-Perot BICs are merged into a super-BIC [61]. Unlike photonic systems, they happen in the geometrical parameter space instead of the momentum space [52], significantly relaxing the fabrication requirement of realizing high-Q acoustic resonances.

This work demonstrates that merging BICs can be realized even in a *single* acoustic resonator. We show that an SP BIC and an FW BIC can be supported simultaneously in a single coupled waveguide-resonator system with different geometric dimensions. Such two BICs experience moving toward each other and merging into a super-BIC as the aspect ratio of the resonator changes. Unlike normal SP BICs and FW BICs, the Q-factor of merged BIC is proportional to ΔL^{-4}, where ΔL is the structure perturbation. We also propose a simple theory based on two- and three-level approximations of the effective non-Hermitian Hamiltonian to account for the physical mechanism of such unique phenomena. Finally, a series of 3D acoustic coupled waveguide-resonator structures were fabricated, and the moving and merging BICs were demonstrated experimentally by identifying the Fano resonance with the vanished linewidth. Our results may pave the way for developing high-performance acoustic devices requiring high-Q resonances, such as acoustic sources, sound lasers, acoustic sensors, and filters.

2 Methods

2.1 Numerical simulations

The complex eigenvalues of all eigenmodes are performed with the commercial software COMSOL Multiphysics. The reflection and transmission spectra are also simulated with COMSOL. When calculating the complex eigenvalues of resonant modes and reflection/transmission spectrum, perfectly matched layer (PML) boundaries at the two ends of waveguides are applied to mimic acoustic wave propagation in the infinite space. The other exterior boundaries are set as hard boundary.

2.2 Fabrication and measurement

The 3D coupled waveguide-acoustic resonators are fabricated with 3D-printing technology. Reflection spectra of these samples are measured using a Brüel & Kjær type-4206T impedance tube with a diameter of 29 mm. The plane wave is generated by a loudspeaker. The amplitude and phase of local pressure are measured by four 1/4-inch condenser microphones (Brüel & Kjær type-4187) situated at designated positions.

3 Results and discussion

3.1 Merged BIC in 2D coupled acoustic resonators

We start by investigating the eigenmodes in a 2D coupled waveguide-resonator system, as shown in Figure 1(a). For the sake of simplicity, the waveguide width is fixed as w =5 cm. If we fix the height of the resonator as H=12 cm but vary the resonator width L from 11 cm to 13 cm, we found that there are two BICs for the same eigenmode M_{13}, whose eigenfield distributions are shown in Figure 1(b, c). Although both BICs share similar features in spatial eigenfields, the eigenfields near the top boundary exhibit different distributions, namely convex and concave for the two BICs, if we closely examine the eigenfield distributions. Further decreasing the height of the resonator and tuning its width simultaneously makes these two BICs approach each other until they merge at H=10.78 cm. This exotic phenomenon reminds us of the merging BIC in a photonic crystal slab, where multiple topological charges tend to merge into Γ point in the first Brillouin zone when structure parameters are delicately tuned. However, merged BICs in the present work happen in the geometry space instead of the momentum space. Note that in our recent work [61], merging FP-BICs has been found in a coupled waveguide-resonator system, where the coupling between two identical resonators plays a vital role in forming merging BICs. Nevertheless, such merging BICs do exist in a single resonator. The merging behavior is confirmed by fitting the Q-factor of BICs as a function of structural perturbation away from the critical position. For normal BIC, its Q-factor is proportional to ΔL^{-2} ($\Delta L=L-L_0$), where L_0 indicates the critical width forming BICs. For merged BIC, the Q-factor is proportional to ΔL^{-4}. These have been verified in Figure 1(d-f). The advantage of merged BICs over normal BICs lies in the fact that its Q-factor is more stable and robust against fabrication imperfections. We also confirmed the moving and merging behaviors of BICs in the reflection spectra mapping in Figure 1(g-i). Note that M_{13} is not the only mode that shows the merging effect on BICs. More examples can be found in the supporting information (see Figures S1 and S2). It is also worth pointing out that such merging BICs can be constructed in a single-port system by leveraging mirror effect, as shown in Figure S3. The merging process of BICs can be well explained from a topological perspective. Each BIC can be linked with a pair of topological charges q=+1 and q=−1 [61-63] for a single port system. When two BICs approach each other, the central two topological charges q=+1 and q=−1 become close until they annihilate. Merging BICs hap-

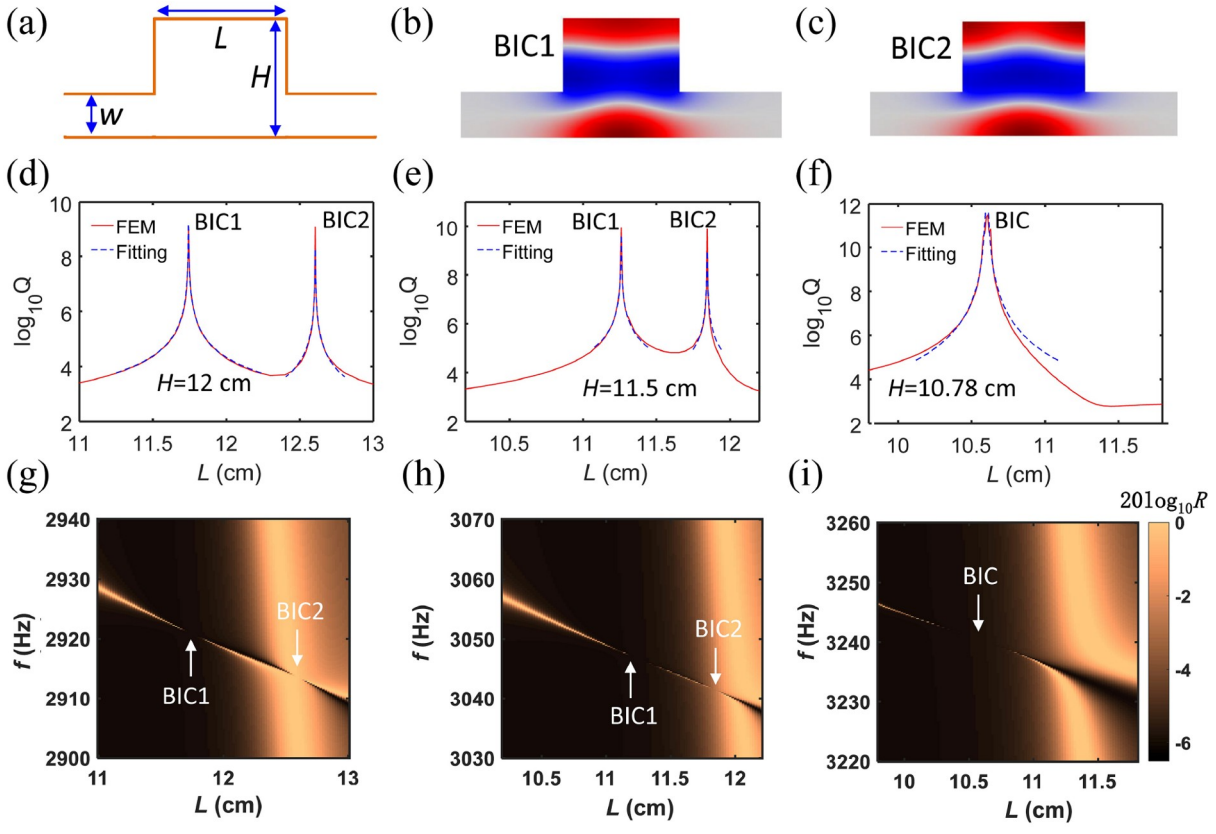

Figure 1 (Color online) (a) Schematic illustration of a coupled waveguide-cuboid resonator system. (b, c) Eigenfield distributions of two BICs at L =11.74 cm and L=12.605 cm with a fixed H=12 cm. (d-f) Q-factors of eigenmodes M_{13} versus L as H is varied from 12 cm to 10.78 cm. Note that the Q-factors of BICs in (d, e) are proportional to ΔL^{-2} ($\Delta L=L-L_0$), while the Q-factor of merged BIC in (f) are proportional to ΔL^{-4} ($\Delta L=L-L_0$). (g-i) Reflection mapping spectra as functions of L and frequency for H=12 cm, 11.5 cm and 10.78 cm.

pens when these two charges annihilate. Detailed discussions can be found in section 1 of supplementary materials and Figures S3-S6.

3.2 Physical mechanism of the merged BICs

To explore its physical mechanism, we perform the modal decomposition to extract the modal expansion coefficients of eigenmodes in a closed rectangular resonator, which form the complete orthogonal eigenbasis. Note that the eigenmodes in a closed resonator are defined as M_{mn}, where m and n are the antinode number in the press field along x-axis and y-axis, respectively. Without loss of generality, we assume the width of waveguide as w=1, and define L_x=L/w and L_y=H/w. By applying the Neuman-boundary-conditions, both of the eigenfrequencies and eigenfunctions of these eigenmodes M_{mn} can be obtained analytically,

$$\frac{\nu_{mn}^2}{\omega_0^2} = \frac{(m-1)^2}{L_x^2} + \frac{(n-1)^2}{L_y^2}, \tag{1a}$$

$$\psi_{mn}(x,y) = \sqrt{\frac{(2-\delta_{m,1})(2-\delta_{n,1})}{L_x L_y}} \cos\left[\frac{\pi(m-1)x}{L_x}\right] \times\cos\left[\frac{\pi(n-1)y}{L_y}\right], \tag{1b}$$

where ν_{mn} is the resonant frequency of eigenmodes M_{mn}, $\omega_0 = \frac{\pi\upsilon}{w} = \pi\upsilon$ is the normalized frequency, and υ is the velocity of sound in the air.

The propagating wave numbers k_p and eigenfunction in the waveguide are given by

$$\frac{\nu^2}{\omega_0^2} = \frac{k_p^2}{\pi^2} + (p-1)^2 (p = 1, 2, 3\ldots), \tag{2a}$$

$$\phi_p(x,y) = \sqrt{\left(2-\delta_{p,1}\right)}\cos[\pi(p-1)y]e^{ik_p x}, \tag{2b}$$

where ν *is* the frequency of propgating wave, p is the antinode number of pressure field perpendicular to the axis of waveguide. The eigenfunction of each BIC in a coupled-waveguided resnator system can be decomposed as

$$\phi_{BIC}(x,y) = \sum_{mn} a_{mn}\psi_{mn}(x,y), \tag{3}$$

where $\psi_{mn}(x,y)$ is the eigenfunction of eigenmodes M_{mn} in a closed resonator and a_{mn} is the modal expansion coefficient.

Figure 2(a, b) shows the modal expansion coefficients of two BICs for structures shown in Figure 1(d), which correspond to peaks of Q-factor at L_x=L/w=2.349 and L_x=L/w=2.537. Figure 2(c) shows the case of merging BICs with structural parameters shown in Figure 1(f). It can be clearly seen that the eigenmode M_{13} of the resonator plays a pivotal role while eigenmodes M_{31}, M_{32}, M_{33} contribute less.

We first consider merged BICs in a two-mode approximation with the participation of two eigenmodes M_{13} and

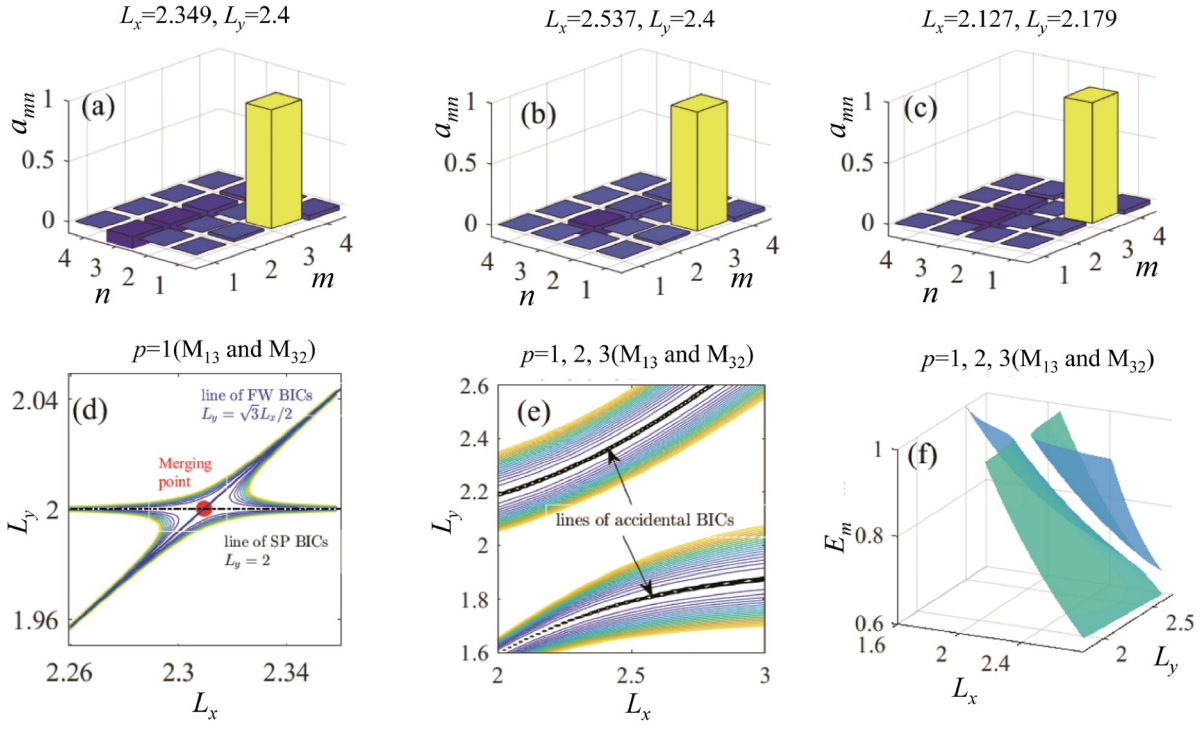

Figure 2 (Color online) (a)-(c) Modal expansions coefficients a_{mn} of eigenmodes by performing modal decomposition on BICs shown in Figure 1 with structural parameters given above, where m and n are antinode numbers of pressure field of mode M_{mn} along x-axis and y-axis, respectively. Contours of resonance width vs sizes of the resonator in two-level approximation without (d) and with (e) account for evanescent modes. Note that the contour color indicates the resonance linewidth. (f) The eigenfrequencies E_m of the resonator that are modified by evanescent modes.

M_{32}. The effective Hamiltonian takes the generic form described in Refs. [18,64]

$$H_{eff}=\begin{pmatrix}\varepsilon-\mathrm{i}\gamma_1 & -\mathrm{i}\sqrt{\gamma_1\gamma_2}\\ -\mathrm{i}\sqrt{\gamma_1\gamma_2} & -\epsilon\varepsilon-\mathrm{i}\gamma_2\end{pmatrix}, \tag{4}$$

where

$$\varepsilon=\frac{\nu_{13}-\nu_{32}}{2}, \tag{5a}$$

$$\gamma_1=W_{13,p=1}^2,\ \gamma_2=W_{32,p=1}^2, \tag{5b}$$

where ν_{13} and ν_{32} are the eigenfrequency of M_{13} and M_{32} in a closed resonator. In what follows, we substitute the eigenfrequency of BIC as this frequency.

In this description, we only keep the first open channel p=1. The coupling constants in Eq. (5b) take the following forms:

$$\begin{aligned}W_{13,p=1}&=\frac{1}{\pi}\sqrt{\frac{L_y}{2L_x}}\sin\left(\frac{2\pi}{L_y}\right),\\ W_{32,p=1}&=\frac{2}{\pi}\sqrt{\frac{L_y}{L_x}}\sin\left(\frac{\pi}{L_y}\right).\end{aligned} \tag{6}$$

Solving the effective non-Hermitian Hamiltonian matrix gives us the complex eigenvalue z,

$$z=-\mathrm{i}\frac{\gamma_1+\gamma_2}{2}\pm\sqrt{\epsilon\varepsilon^2-\left(\frac{\gamma_1+\gamma_2}{2}\right)^2-\mathrm{i}\epsilon\varepsilon(\gamma_1-\gamma_2)}\,. \tag{7}$$

The real and imaginary parts of the eigenvalue correspond to the resonant peak position and resonant linewidth, respectively [65]. The Q-factor is defined as $Q=-Re(z)/2Im(z)$. BIC happens at $Im(z)=0$ as the resonance has an infinite Q-factor. That occurs for two cases, $\gamma_1=0$ or $\varepsilon=0$. The first case occurs if $W_{13,\,p=1}$=0 for L_y=2 according to Eq. (6) which clearly defines the eigenmode M_{13} as the SP BIC with the normalized frequency $\nu_c=2/L_y=1$. The second case gives us the FW BIC [17,25,28,44] for $\nu_{13}=\nu_{32}$ or $L_y=\sqrt{3}L_x/2$ with the frequency $2/L_y$. Since BICs always happen around intesecting frequency ($L_y=\sqrt{3}L_x/2$), we introduce a small perturbation as $L_y=\frac{\sqrt{3}L_x}{2}+\xi$, where ξ is a perturbation parameter close to 0. Moreover, SP BIC happens only when $W_{13,\,p=1}$=0, corresponding to L_y=2. We can apply a small perturbation by setting L_y=2+y to study the mode property of acoustic resonances nearby the critical value. To inteprete the merging behavior of SP BICs and FW BICs, we need introduce both perturabtions L_y=2+y and $L_y=\frac{\sqrt{3}L_x}{2}+\xi$. Substituting them into Eqs. (5) and (7) gives us

$$\epsilon\varepsilon\approx\frac{\sqrt{3}}{L_xL_y}\xi,\ \gamma_1\approx\frac{y^2}{4L_x}. \tag{8}$$

Therefore, the eigenvalue responsible for BICs can be presented as

$$z\approx\frac{\sqrt{3}}{L_xL_y}\xi+\mathrm{i}Ay^2\xi^2, \tag{9}$$

where A is an irrelevant constant. Figure 2(d) shows the contours of the imaginary part of this eigenvalue. Thus, the merging point is the saddle point at which the SP BIC with the Q-factor $Q\sim1/\left(L_y-2\right)^2$ coalesces with the FW BIC with $Q\sim1/\left(L_y-\sqrt{3}L_x/2\right)^2$ as plotted in Figure 2(d). However, the frequency of SP BIC equals the cutoff frequency of the second continuum at ν=1, while numerical simulation shows the BICs frequencies are below the cut-off frequency. Thus, we shall consider the evanescent modes (closed channels), which modify the effective Hamiltonian as follows

$$H_{eff}=\begin{pmatrix}\epsilon\varepsilon'-\mathrm{i}\gamma_1 & u-\mathrm{i}\sqrt{\gamma_1\gamma_2}\\ u-\mathrm{i}\sqrt{\gamma_1\gamma_2} & -\epsilon\varepsilon'-\mathrm{i}\gamma_2\end{pmatrix}, \tag{10}$$

where

$$\varepsilon'=\frac{\nu_{13}-\nu_{32}}{2}+\sum\nolimits_{p>1}\left|k_p\right|\left(W_{13,p}^2-W_{32,p}^2\right), \tag{11a}$$

$$u=\sum\nolimits_{p>1}\left|k_p\right|W_{13,p}W_{32,p}. \tag{11b}$$

In this case, Figure 2(e) shows that the merging effect disappears because the evanescent modes modify the Hamiltonian of the closed resonator

$$H_m=\begin{pmatrix}\epsilon\varepsilon' & u\\ u & -\epsilon\varepsilon'\end{pmatrix}. \tag{12}$$

Such a Hamiltonian gives rise to a repulsion of the former eigenfrequencies of the closed resonator. As a result, the eigenfrequencies $\epsilon\varepsilon'$ cannot turn to zero and realize the FW BICs, as seen in Figure 2(f). Notice that another combination of the eigenmodes, for example, the modes M_{13} and M_{31} or M_{13} and M_{33} gives rise to the same results: merging of SP BIC and FW BIC without evanescent modes and absence of merging with account of evanescent modes of waveguide. Therefore, we can conclude that the widely accepted two-level approximation of BICs is insufficient to describe the merging of SP BICs with the FW BICs. That was shown for consideration of multichannel BICs [66].

Indeed, modal decomposition shows in Figure 2(a-c) that modes M_{31}, M_{32}, M_{33} contribute equally to BIC besides the dominant contribution of M_{13}. Therefore, we try to expand the effective Hamiltonian by incorporating three eigenmodes M_{13}, M_{31}, M_{32}. Figure 3(a) shows that in this case two eigenfrequencies modified by evanescent modes are crossing to resume the FW BIC, which merge with the SP BIC, as illustrated in Figure 3(b). Figure 3(c, d) shows the merging in transmission spectra mapping with a variation of the width of the resonator. Thus, the merging BICs in an open resonator is well captured by a three-level system.

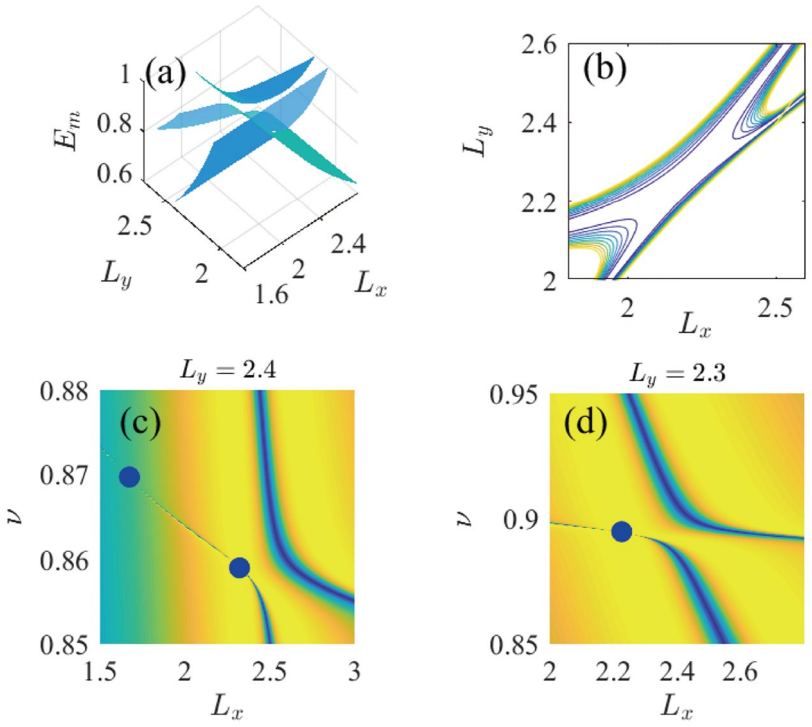

Figure 3 (Color online) (a) The eigenfrequencies of resonator modified by evanescent modes in the three-level description M_{13}, M_{32}, and M_{31}. (b) Contours of resonant width vs sizes of the resonator. (c) and (d) Transmittance vs length of resonator and frequency. Closed blue circles mark BICs.

3.3 Experimental demonstration of merging BICs in a 3D open resonator

Next, we move to the experimental demonstration of such merging BICs. In the actual implementation, we consider a cylindrical waveguide with a diameter of 29 mm, and a side resonator with a fixed width of 29 mm is attached to it. The length L_x and height H are chosen as variables to observe the moving BICs. Figure 4(a) shows the experimental setup of the measurement system. It is not surprising that there are two BICs for the same mode M_{113}, as demonstrated in Figure 4(b, c), when we scan the length L_x at a fixed H. Moreover, we can find that two BICs gradually approach each other when H varies from 52 mm to 40 mm. Here, it is necessary to point out that further reducing H increases the resonant frequency above the cut-off frequency. Thus we cannot observe truly merging BICs in such a realistic system. However, one can still see these two BICs become closer to each other as we decrease H. They still show a merging effect but not in the form of an ideal BIC. To corroborate these findings, we fabricate a series of samples with 3D printing technology. Figure 4(d-f) shows the measured transmission spectra mapping as functions of frequency and L_x for H=52 mm, 48 mm, and 44 mm, respectively. To make a comparison, we also calculate the simulated transmission spectra mapping for these structures shown in Figure 4(g-i). Excellent agreements can be found between experiments and simulations. Besides, we indeed observe that two BICs appear at H =52 mm, which are manifested by the resonance linewidth vanishing. These two BICs move to each other as H decreases. To better visualize the position of BICs and their moving trend, transmission spectra at different L_x for H =52 mm, 48 mm, and 44 mm, are plotted and shown in Figure S7.

4 Conclusion

We reveal that merging BICs can be constructed in an acoustic open resonator by varying the aspect ratio of the resonator. We show that two types of BICs, including SP BICs and FW BICs, can be supported for the same mode for a resonator with a fixed height but a varied width. They move toward each other until they merge into a single super-BIC as the aspect ratio of the resonator changes. The merged BICs show better stability than the normal SP BICs and FW BICs because their Q-factors are less sensitive to structure perturbations as compared to their counterparts, with an improvement from ΔL^{-2} to ΔL^{-4}. Such an exotic phenomenon is well explained by the two- and three-level approximations of the effective non-Hermitian Hamiltonian. Finally, we demonstrate these interesting findings experimentally in a 3D coupled waveguide-resonator system. The evolutions and approaching of two BICs are confirmed by checking two Fano resonances with vanished linewidth. Our results may

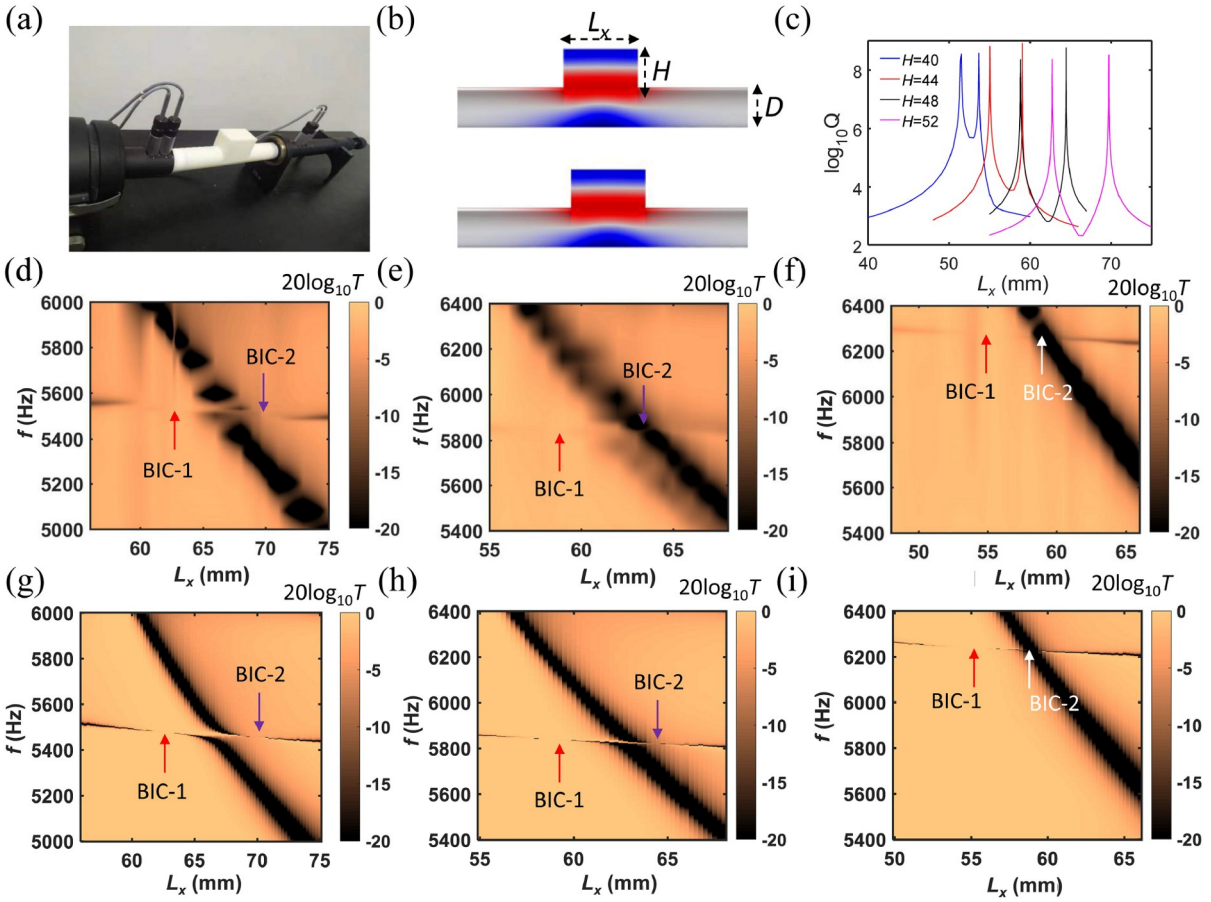

Figure 4 (Color online) (a) Photograph of 3D coupled-waveguide resonator system fabricated by 3D-printing. (b) Eigenfield distributions of two BICs. (c) Q-factors of mode M_{131} versus L_x at different H. (d-f) Measured transmission spectra mapping as functions of L_x and frequency at H=52 mm (d), H=48 mm (e), and H=44 mm (f). (g-i) Simulated transmission spectra mapping as functions of L_x and frequency at H=52 mm (g), H=48 mm (h), and H=44 mm (i).

hold great promise in enhanced wave-matter interactions.

Note: Prof. Almas F. Sadreev, one of the corresponding authors, passsed away during the review process of this work. We would like to dedicate this work to him.

Bin Jia, Sibo Huang, and Yong Li are supported by the National Natural Science Foundation of China (Grant No. 12074286), and Shanghai Science and Technology Committee (Grant No. 21JC1405600). Andrey E. Miroshnichenko is supported by the Australian Research Council Discovery Project (Grant No. DP200101353). Almas F. Sadreev is supported by Russian Science Foundation (Grant No. 22-12-00070).

Conflict of interest The authors declare that they have no conflict of interest.

Supporting Information

The supporting information is available online at http://phys.scichina.com and https://link.springer.com. The supporting materials are published as submitted, without typesetting or editing. The responsibility for scientific accuracy and content remains entirely with the authors.

1 C. W. Hsu, B. Zhen, A. D. Stone, J. D. Joannopoulos, and M. Soljačić, Nat. Rev. Mater **1**, 16048 (2016).
2 A. F. Sadreev, Reports Prog. Phys. **84**, 55901 (2021).
3 L. Huang, L. Xu, D. A. Powell, W. J. Padilla, and A. E. Miroshnichenko, Phys. Rep. **1008**, 1 (2023).
4 K. Koshelev, G. Favraud, A. Bogdanov, Y. Kivshar, and A. Fratalocchi, Nanophotonics **8**, 725 (2019).
5 L. Huang, L. Xu, M. Woolley, and A. E. Miroshnichenko, Adv. Quantum Tech. **3**, 1900126 (2020).
6 J. Wang, P. Li, X. Zhao, Z. Qian, X. Wang, F. Wang, X. Zhou, D. Han, C. Peng, L. Shi, and J. Zi, Photonics Insights **3**, R01 (2024).
7 M. Kang, T. Liu, C. T. Chan, and M. Xiao, Nat. Rev. Phys. **5**, 659 (2023).
8 L. Huang, S. Huang, C. Shen, S. Yves, A. S. Pilipchuk, X. Ni, S. Kim, Y. K. Chiang, D. A. Powell, J. Zhu, Y. Cheng, Y. Li, A. F. Sadreev, A. Alù, and A. E. Miroshnichenko, Nat. Rev. Phys. **6**, 11 (2024).
9 M. Zhou, S. You, L. Xu, M. Fan, J. Huang, W. Ma, M. Hu, S. Luo, M. Rahmani, Y. Cheng, L. Li, C. Zhou, L. Huang, and A. E. Miroshnichenko, Sci. China-Phys. Mech. Astron. **66**, 124212 (2023).
10 S. Feng, T. Liu, W. Chen, F. Wu, and S. Xiao, Sci. China-Phys. Mech. Astron. **66**, 124214 (2023).
11 M. Bolsterli, Phys. Rev. **182**, 1095 (1969).
12 M. Robnik, J. Phys. A-Math. Gen. **19**, 3845 (1986).
13 R. L. Schult, D. G. Ravenhall, and H. W. Wyld, Phys. Rev. B **39**, 5476 (1989).
14 N. Moiseyev, Phys. Rev. Lett. **102**, 167404 (2009).
15 D. Evans, Q. J. Mech. Appl. Math. **51**, 263 (1998).
16 B. Jia, L. Huang, A. S. Pilipchuk, S. Huang, C. Shen, A. F. Sadreev, Y. Li, and A. E. Miroshnichenko, Phys. Rev. Appl. **19**, 54001 (2023).
17 H. Friedrich, and D. Wintgen, Phys. Rev. A **32**, 3231 (1985).

18 A. F. Sadreev, E. N. Bulgakov, and I. Rotter, Phys. Rev. B **73**, 235342 (2006).
19 M. V. Rybin, K. L. Koshelev, Z. F. Sadrieva, K. B. Samusev, A. A. Bogdanov, M. F. Limonov, and Y. S. Kivshar, Phys. Rev. Lett. **119**, 243901 (2017).
20 L. Huang, L. Xu, M. Rahmani, D. Neshev, and A. E. Miroshnichenko, Adv. Photon. **3**, 016004 (2021).
21 C. M. Linton, M. McIver, P. McIver, K. Ratcliffe, and J. Zhang, Wave Motion **36**, 67 (2002).
22 Y. Duan, W. Koch, C. M. Linton, and M. McIVER, J. Fluid Mech. **571**, 119 (2007).
23 S. Hein, and W. Koch, J. Fluid Mech. **605**, 401 (2008).
24 S. Hein, W. Koch, and L. Nannen, J. Fluid Mech. **664**, 238 (2010).
25 L. Huang, B. Jia, A. S. Pilipchuk, Y. Chiang, S. Huang, J. Li, C. Shen, E. N. Bulgakov, F. Deng, D. A. Powell, S. A. Cummer, Y. Li, A. F. Sadreev, and A. E. Miroshnichenko, Phys. Rev. Appl. **18**, 54021 (2022).
26 S. Huang, T. Liu, Z. Zhou, X. Wang, J. Zhu, and Y. Li, Phys. Rev. Appl. **14**, 21001 (2020).
27 T. Lepetit, and B. Kanté, Phys. Rev. B **90**, 241103 (2014).
28 L. Huang, Y. K. Chiang, S. Huang, C. Shen, F. Deng, Y. Cheng, B. Jia, Y. Li, D. A. Powell, and A. E. Miroshnichenko, Nat. Commun. **12**, 4819 (2021).
29 A. S. Pilipchuk, and A. F. Sadreev, Phys. Lett. A **381**, 720 (2017).
30 H. Friedrich, and D. Wintgen, Phys. Rev. A **31**, 3964 (1985).
31 C. W. Hsu, B. Zhen, J. Lee, S. L. Chua, S. G. Johnson, J. D. Joannopoulos, and M. Soljačić, Nature **499**, 188 (2013).
32 D. C. Marinica, A. G. Borisov, and S. V. Shabanov, Phys. Rev. Lett. **100**, 183902 (2008).
33 E. N. Bulgakov, and A. F. Sadreev, Phys. Rev. A **90**, 53801 (2014).
34 C. Zhou, L. Huang, R. Jin, L. Xu, G. Li, M. Rahmani, X. Chen, W. Lu, and A. E. Miroshnichenko, Laser Photonics Rev. **17**, 2200564 (2023).
35 S. A. Cummer, J. Christensen, and A. Alù, Nat. Rev. Mater. **1**, 16001 (2016).
36 B. Assouar, B. Liang, Y. Wu, Y. Li, J. C. Cheng, and Y. Jing, Nat. Rev. Mater **3**, 460 (2018).
37 G. Ma, and P. Sheng, Sci. Adv. **2**, e1501595 (2016).
38 Y. Cheng, C. Zhou, B. G. Yuan, D. J. Wu, Q. Wei, and X. J. Liu, Nat. Mater. **14**, 1013 (2015).
39 X. Zhu, B. Liang, W. Kan, Y. Peng, and J. Cheng, Phys. Rev. Appl. **5**, 54015 (2016).
40 Z. Yang, J. Mei, M. Yang, N. H. Chan, and P. Sheng, Phys. Rev. Lett. **101**, 204301 (2008).
41 Z. Zhou, S. Huang, D. Li, J. Zhu, and Y. Li, Natl. Sci. Rev. **9**, nwab171 (2022).
42 S. Huang, Z. Zhou, D. Li, T. Liu, X. Wang, J. Zhu, and Y. Li, Sci. Bull. **65**, 373 (2020).
43 S. Hein, W. Koch, and L. Nannen, J. Fluid Mech. **692**, 257 (2012).
44 A. A. Lyapina, D. N. Maksimov, A. S. Pilipchuk, and A. F. Sadreev, J. Fluid Mech. **780**, 370 (2015).
45 I. Deriy, I. Toftul, M. Petrov, and A. Bogdanov, Phys. Rev. Lett. **128**, 84301 (2022).
46 F. Kronowetter, M. Maeder, Y. K. Chiang, L. Huang, J. D. Schmid, S. Oberst, D. A. Powell, and S. Marburg, Nat. Commun. **14**, 6847 (2023).
47 Z. Zhou, B. Jia, N. Wang, X. Wang, and Y. Li, Phys. Rev. Lett. **130**, 116101 (2023).
48 H. Zhang, S. Liu, Z. Guo, S. Hu, Y. Chen, Y. Li, Y. Li, and H. Chen, Sci. China-Phys. Mech. Astron. **66**, 284311 (2023).
49 S. Huang, S. Xie, H. Gao, T. Hao, S. Zhang, T. Liu, Y. Li, and J. Zhu, Fundamental Res. **4**, 57 (2024).
50 E. N. Bulgakov, and D. N. Maksimov, Phys. Rev. A **96**, 63833 (2017).
51 L. Yuan, and Y. Y. Lu, Phys. Rev. A **95**, 23834 (2017).
52 E. Bulgakov, A. Pilipchuk, and A. Sadreev, Phys. Rev. B **106**, 75304 (2022).
53 E. Bulgakov, G. Shadrina, A. Sadreev, and K. Pichugin, Phys. Rev. B **108**, 125303 (2023).
54 E. N. Bulgakov, and D. N. Maksimov, Phys. Rev. Lett. **118**, 267401 (2017).
55 Z. Zhang, E. Bulgakov, K. Pichugin, A. Sadreev, Y. Xu, and Y. Qin, Phys. Rev. Appl. **20**, L011003 (2023).
56 J. Jin, X. Yin, L. Ni, M. Soljačić, B. Zhen, and C. Peng, Nature **574**, 501 (2019).
57 M. Kang, S. Zhang, M. Xiao, and H. Xu, Phys. Rev. Lett. **126**, 117402 (2021).
58 M. Kang, L. Mao, S. Zhang, M. Xiao, H. Xu, and C. T. Chan, Light Sci. Appl. **11**, 228 (2022).
59 H. Barkaoui, K. Du, Y. Chen, S. Xiao, and Q. Song, Phys. Rev. B **107**, 45305 (2023).
60 G. Sun, Y. Wang, Y. Li, Z. Cui, W. Chen, and K. Zhang, Phys. Rev. B **109**, 035406 (2024).
61 L. Huang, B. Jia, Y. K. Chiang, S. Huang, C. Shen, F. Deng, T. Yang, D. A. Powell, Y. Li, and A. E. Miroshnichenko, Adv. Sci. **9**, 2200257 (2022).
62 Z. Sakotic, A. Krasnok, A. Alú, and N. Jankovic, Photon. Res. **9**, 1310 (2021).
63 C. Guo, J. Li, M. Xiao, and S. Fan, Phys. Rev. B **108**, 155418 (2023).
64 A. Volya, and V. Zelevinsky, Phys. Rev. C **67**, 54322 (2003).
65 I. Rotter, Rep. Prog. Phys. **54**, 635 (1991).
66 A. S. Pilipchuk, A. A. Pilipchuk, and A. F. Sadreev, Phys. Scr. **94**, 115004 (2019).